Collision-Induced infrared absorption and Raman scattering of H2 in supercritical CO2

Isaline Bonnin, Raphaël Mereau, Karine de Oliveira Vigier, Thierry Tassaing

Collision-Induced Infrared Absorption and Raman scattering of H_2 in supercritical CO_2

Isaline Bonnin,[1,2] Raphaël Mereau,[1] Karine De Oliveira Vigier[2,] Thierry Tassaing,[1]*

[1] Institut des Sciences Moléculaires (ISM), Univ. Bordeaux, CNRS, Bordeaux INP, ISM, UMR 5255, F-33400 Talence, France

[2] Institut de Chimie des Milieux et Matériaux de Poitiers (IC2MP), Univ. de Poitiers, UMR CNRS 7285, 1 rue Marcel Doré, 86073 Poitiers Cedex 9, France

Corresponding author: thierry.tassaing@u-bordeaux.fr

Abstract

In this study, the solvation of H_2 in supercritical CO_2 was investigated by co-localized infrared absorption/Raman scattering spectroscopies. The Fermi dyad and combinations of vibrational modes of CO_2 were detected by Raman and infrared spectroscopy respectively, with increasing intensities according to CO_2 concentrations varying from 1 to 15 mol.L^{-1}. H_2 rotational bands and vibrons with almost constant intensities were detected by Raman spectroscopy according to a constant H_2 pressure of 3 MPa. In contrast, a collision-induced infrared band of H_2 was reported for the first time in supercritical CO_2 and its intensity was found to be directly proportional to the intensity of the CO_2 bands. In addition, the intensities of the H_2 and CO_2 contributions were found to be sensitive to the local density fluctuations existing near the critical temperature of CO_2 (Tc = 31 °C, Pc = 7.4 MPa).

Keywords: Supercritical CO_2, Hydrogen, Collision induced effects, Infrared, Raman

1- Introduction

In order to take into account the environmental concerns due to anthropogenic emissions of carbon dioxide (CO_2) in the atmosphere, many research works on the potential utilization of CO_2 as a key intermediate for chemistry are currently underway [1–4]. In particular, CO_2 is considered as a substantial C1-carbon source to produce chemicals and fuels. In association with hydrogen (H_2), the CO_2 molecule can lead to basic chemicals such as methane, methanol, formic acid, methylal, methyl formate and dimethylether via the CO_2 hydrogenation reaction [5]. For instance, in the pioneering work of Jessop *et al.* [6] the catalytic hydrogenation of CO_2 to formic acid in supercritical CO_2, in which H_2 is highly miscible, was found to be much faster than in liquid organic solvents under identical conditions suggesting that supercritical CO_2 is a promising medium for homogeneous catalysis. We remember that in the vicinity of the critical point, supercritical CO_2 could display an 'hyper-compressible' regime in which the high susceptibility of the density to small pressure variations on a macroscopic scale reflects strong local density fluctuations existing at the molecular level [7–10]. This phenomenon does not have a counterpart in the liquid phase and it has been shown in previous investigations that

these local density enhancements (LDE) might have significant consequences on the solvation and reactivity of a solute in supercritical fluids [11,12].

In this context, the monitoring of supercritical CO_2 and H_2 during the production of various chemicals and fuels is of prime interest for thermodynamic investigations, kinetic studies and mechanisms at work in such processes. To this aim, vibrational spectroscopic methods are powerful tools that are particularly adapted to perform *in situ* and *in operando* investigations. In the case of CO_2-H_2 mixture, both Raman and infrared (IR) spectroscopy might be used to detect both molecules. Thus, it is well known that nonpolar molecules such as H_2 are active in scattering Raman and inactive in IR while CO_2, with its four vibrational modes, can be monitored by both techniques. In order to detect homonuclear diatomic molecules such as H_2 by IR absorption spectroscopy, pressure-induced effect might be used by gas compression or by the addition of a nonpo38lar gas in the system. In the literature, only few authors have reported pressure-induced IR absorption of H_2 [13,14] and, to the best of our knowledge, CO_2 induced effect on H_2 has not been reported yet.

Generally, IR and Raman experiments are performed separately on two different samples using two different optical cells that are specific to both technics. Herein, CO_2-H_2 mixtures were investigated by co-localized IR/Raman spectroscopy analysis. We define co-localized IR/Raman measurement to be the sequential or simultaneous acquisition of IR and Raman spectra using a single high-pressure cell for both spectroscopic measurements during the same experiment. Besides the time advantage, the utilization of a single high-pressure cell for the co-localized collection of Raman and IR spectroscopic data allows a direct comparison of the IR and Raman data and avoids any possible experimental errors related to the reproducibility of the experimental conditions when independent IR and Raman experiments are performed.

Thus, the aim of this work is to use co-localized IR/Raman spectroscopies in a single high-pressure cell for the *in situ* monitoring of H_2 in supercritical CO_2. Experiments were performed with 3 MPa of H_2 diluted in CO_2 with increasing CO_2 concentrations from 1 to 15 mol.L^{-1} at 36 and 60°C. The evolution of the intensity of selected vibrational modes of CO_2 and H_2 detected by both Raman and IR spectroscopies have been analyzed as a function of the CO_2 concentrations. Thus, a collision-induced IR spectrum of H_2 in supercritical CO_2 is clearly put in evidence. On the other hand, the effect of the local density fluctuations existing near the critical temperature of CO_2 on the intensities of the IR and Raman spectra of H_2 and CO_2 are discussed.

2- Experimental

The *in situ* analysis of the CO_2-H_2 mixture by the combination of IR and Raman spectroscopy was done in one high-pressure cell (**Fig. 1**). The home-made stainless-steel cell is composed of three cylindrical windows (one sapphire window for Raman scattering and two silicon windows for IR absorption with a pathlength of 26 mm). Windows were positioned on the flat surface of an inconel plug with a Teflon foil placed between the window and the plug-in to compensate for imperfections at the two surfaces (unsupported area principle). Flat Teflon rings were used to ensure sealing between the plug and the cell body. The heating was achieved using four cartridge heaters disposed in the body of the cell and a thermocouple located close to one

cartridge was used to regulate the temperature at 36 or 60°C with an accuracy of about $\Delta T = \pm$ 0.5°C. The cell was connected via a stainless capillary to a pressurizing system which permits the regulation of pressure with an accuracy of about $\Delta P = \pm$ 0.01 MPa.

Prior to all experiments, the cell was vacuumed at least 15 min to remove atmospheric gases and in particular water. Then, experiments were performed by adding firstly 3 MPa of H_2 (purchased from Air Liquid (99.9999 % purity)) in the high-pressure cell heated at 36 or 60°C. CO_2 (purchased from Air Liquid (99.95 % purity)) was then added in the high-pressure cell using a manual pump (TOP industrie) up to the desired pressure. **Table 1** describes the range of CO_2 pressures and corresponding CO_2 concentrations investigated in this study.

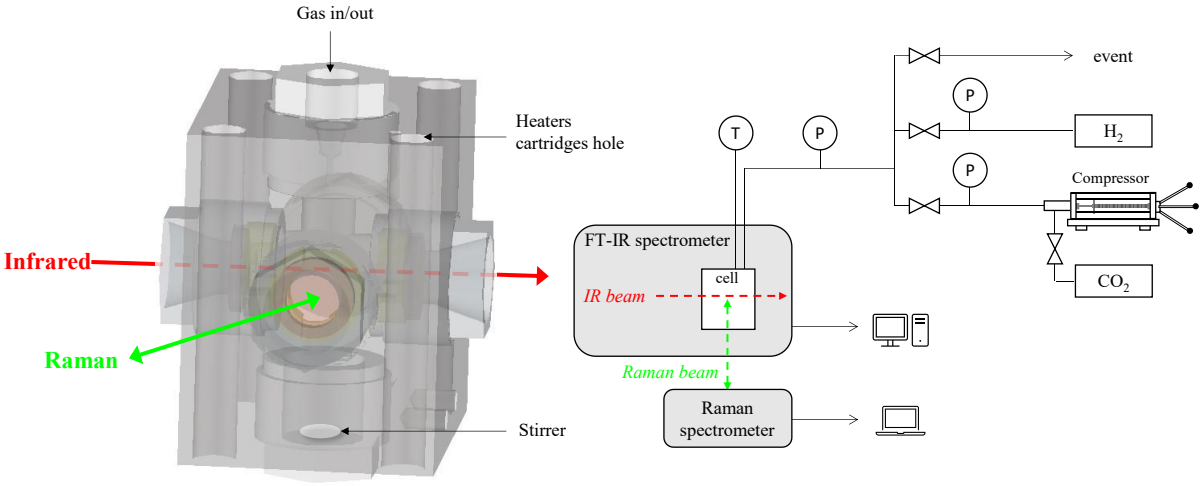

Figure 1: Design of the high-pressure experimental device with a single high-pressure cell coupled with IR and Raman spectrometer for the *in situ* measurements of the CO_2-H_2 mixture.

For IR absorption measurements, a Nicolet 6700 FTIR spectrometer equipped with a Globar source, a KBr/Ge beamsplitter and a DLaTGS/KBr thermal detector was used to investigate the spectral range from 400 to 6500 cm^{-1}. Single beam spectra with 4 cm^{-1} resolution were obtained by Fourier transformation of 100 accumulated interferograms in order to improve the signal to noise ratio. In that region, fundamental and combination bands of CO_2 were observed but only the spectral range between 3800 and 5200 cm^{-1} was analyzed and of interest for our purpose under our experimental conditions. In particular, the strong absorption of CO_2 precludes any quantitative analysis outside this spectral range and only the less intense bands of CO_2 were integrated from 4900 to 4760 cm^{-1} and from 5200 to 5035 cm^{-1} for the quantitative analysis performed in this study (see below). In the same manner, the collision-induced IR spectral band of H_2 that is observed at about 4150 cm^{-1} was integrated from 4585 to 4000 cm^{-1} for the quantitative analysis of induced effect on the H_2 molecule.

For Raman scattering measurements, a portable home-made spectrometer was used and equipped with a laser diode DJ532-40 (Thorlabs) (532 nm – 40 mW) as the laser source and a custom-made USB 2000 spectrometer from Ocean Optics (grating: 1200 lines/mm, slit: 25 µm, CCD detector 2048 pixels) to reach the spectral range between 200 and 4250 cm^{-1} with a spectral resolution between 8 and 4 cm^{-1} (about 6 cm^{-1} at 1000 cm^{-1}). Each spectrum results from the average of 2 accumulated scans with an integration time for each scan of about 30 seconds. Fermi dyad of CO_2 were detected at about 1284 cm^{-1} and 1387 cm^{-1} and they were

both integrated from 1200 to 1500 cm^{-1} for the quantitative analysis. Several rotational bands of H_2 were observed in the spectral range between 300 and 1200 cm^{-1} but only the more intense one at 581 cm^{-1} was integrated from 535 to 640 cm^{-1}. Some fluorescence peaks of the sapphire window in the region from approximately 100 to 500 cm^{-1} were also recorded as a background spectrum before CO_2 and H_2 insertion in the cell.

Table 1: CO_2 pressures and their corresponding concentrations added in the high-pressure cell containing already 3 MPa of H_2. The concentrations of CO_2 are obtained from the NIST Chemistry Webbook [15,16].

36°C		60°C	
Pressure (MPa)	Concentration ($mol.L^{-1}$)	Pressure (MPa)	Concentration ($mol.L^{-1}$)
0.78	0.31	0.90	0.33
2.66	1.19	2.90	1.17
4.33	2.18	4.90	2.18
5.22	2.83	6.00	2.84
6.40	4.00	7.61	4.01
7.10	5.06	8.74	5.07
7.53	6.02	9.57	6.02
7.78	6.85	10.20	6.89
8.00	8.06	10.96	8.06
8.20	10.12	12.15	10.13
8.40	12.34	13.70	12.41
8.80	14.03	15.35	14.01
9.60	15.44	17.70	15.47

3- Results and discussion

3-1 Infrared and Raman study of H_2 diluted in supercritical CO_2

The IR and Raman spectra of the H_2-CO_2 mixtures at a constant pressure of H_2 (3 MPa) were measured at 36 and 60 °C for the same increasing concentration values of supercritical CO_2 (see **Table 1**) using a single high-pressure cell for the simultaneous acquisition of the IR and Raman spectra on the same sample. **Figure 2a and 2c** show the IR and Raman spectra respectively, recorded at 36°C for increasing CO_2 pressures from 0.8 to about 10 MPa. The overview IR spectra of the spectral range from 3900 to 5200 cm^{-1} in **Figure 2a** displays three peaks at 4850, 4980 and 5100 cm^{-1} that are assigned to the combination modes $4\nu_2 + \nu_3$, $\nu_1 + 2\nu_2 + \nu_3$ and $2\nu_1 + \nu_3$ of CO_2 respectively [17]. As expected, their intensities are increasing according to CO_2 pressure. By the same token, a broad band is observed at 4140 cm^{-1} that also increases according to the CO_2 pressure. Such band can be assigned to the collision-induced IR absorption of H_2 that has been reported previously for H_2 diluted in monoatomic gases under high pressure conditions [13,14]. To the best of our knowledge, the collision-induced IR spectrum of H_2 in supercritical CO_2 has not been reported previously. An enlarged view on the absorption IR profile associated with the stretching vibration of H_2 in the spectral range from 3900 to 4600 cm^{-1} is reported in **Figure 2b**. The band-shape is composed of two maxima at 4150 and 4200 cm^{-1} respectively labelled as Q_p and Q_r that are characteristics of the collision-induced IR spectrum of H_2 [14],[18]. As the CO_2 pressure is increasing, the intensity of the whole profile is increasing and the dip between Q_p and Q_r bands is filling up while we do not observe any significant frequency shift of the whole profile. Similarly, we did not observe any variation of the width of the band in the temperature and pressure range investigated.

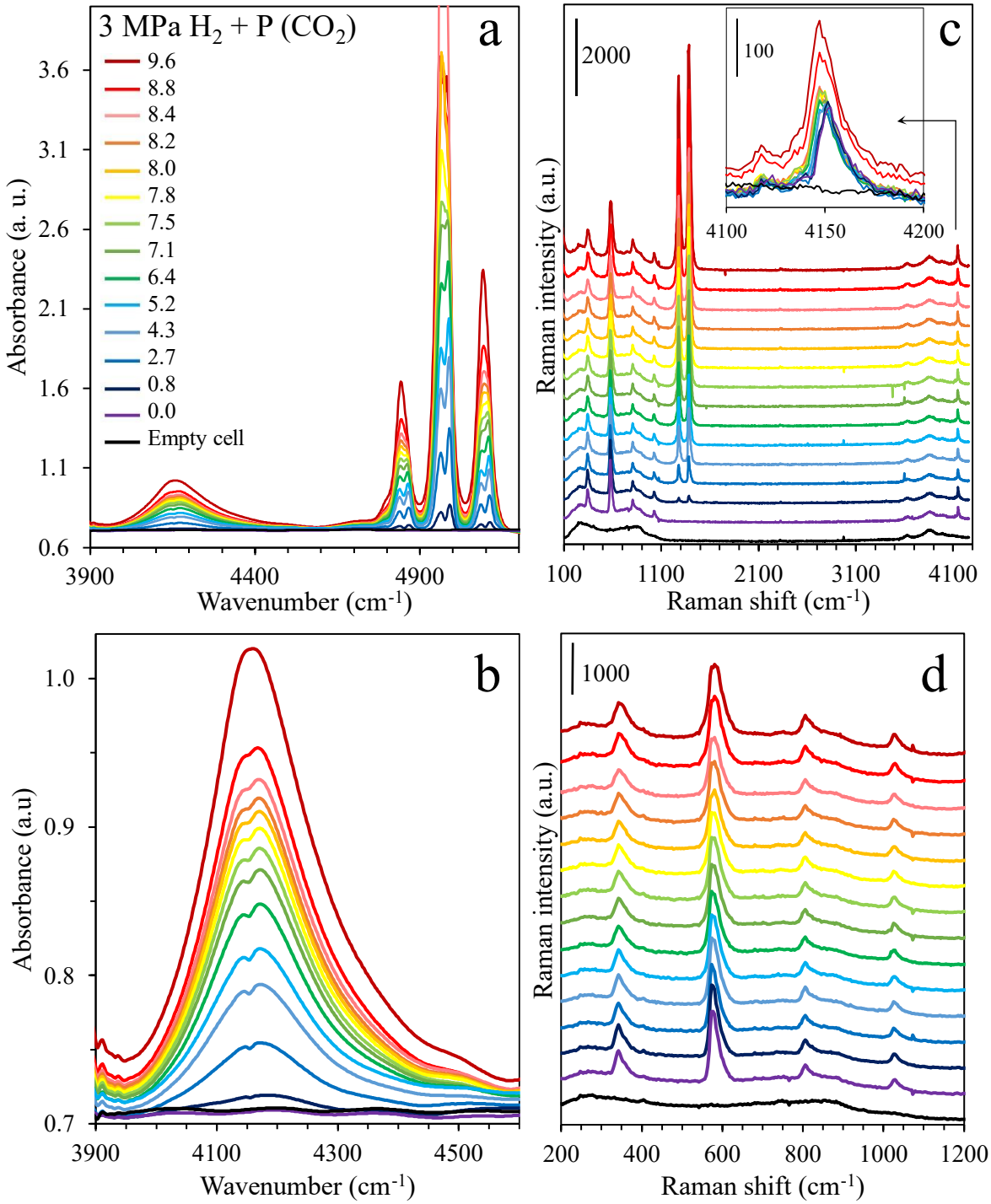

Figure 2: Co-localized IR absorption (top left) and Raman (top right) spectra of the H_2-CO_2 mixture at 36°C with 3 MPa of H_2 and various CO_2 pressure. Enlarged view of the H_2 peaks (bottom).

Figure 2c shows the Raman spectra of the H_2-CO_2 mixture recorded from 100 to 4300 cm^{-1} at 36°C for increasing CO_2 pressures from 0.8 to about 10 MPa and an enlarged view on the lower frequency region between 200 and 1200 cm^{-1} is displayed on **Figure 2d**. The Raman spectrum of the empty cell spectrum displays two broad bands from approximately 150 to 1000 cm^{-1} and from 3500 to 4100 cm^{-1} that are related to the fluorescence contribution of the sapphire window. The two bands observed at 1284 and 1387 cm^{-1} are assigned to the Fermi resonance dyad of CO_2 [19–23] and those intensities are proportional to the CO_2 concentration. In the high Raman

shift region that correspond to the ro-vibrational spectrum associated with the stretching vibration of H_2 (also called the vibrons) that is Raman active, we should detect four contributions usually labelled (Q1 (J=0), Q1 (J=1), Q1 (J=2), and Q1 (J=3) at 4160, 4156, 4145 and 4127 cm^{-1}. Under our experimental conditions and in view of the low signal to noise ratio in this spectral range, we observed at 4152 cm^{-1} a main contribution that corresponds to Q_1 (J=1) and a weak peak at about at 4125 cm^{-1} that corresponds to Q_1 (J=3) [24–26]. In the low frequency range, rotational bands of H_2 that are also Raman active are observed at 343, 580, 806 and 1031 cm^{-1} and are related to S_0 branch from the 0 to 3rd rotational level, respectively [24,26,27]. Band shapes and band center frequencies of the Raman spectra of H_2 do not display any significant variation upon an increase of the CO_2 pressure. By the same token, the intensity of the Raman spectra of H_2 is almost constant over the pressure range investigated.

3-2 Analysis of the intensity of the infrared and Raman spectra

In order to compare the evolution of the intensity of the H_2 and CO_2 contribution in both the IR and Raman spectra, we have determined in the IR spectra the integrated area of the H_2 stretching mode at 4150 cm^{-1} and of the combination $4\nu_2 + \nu_3$ and $2\nu_1 + \nu_3$ of CO_2 at 4850 cm^{-1} and 5097 cm^{-1} respectively, and in the Raman spectra, the integrated area of the H_2 rotational band at 580 cm^{-1} and of the fermi dyad of CO_2. The results are reported as a function of the CO_2 concentration at 36 and 60°C in **Figure 3a and 4a** for the IR and Raman spectra respectively. For each temperature, the same concentration values of CO_2 were measured for proper comparison.

In **Figure 3a**, both IR area of the CO_2 and the H_2 contributions increases with the CO_2 concentration and the curves for both the CO_2 and the H_2 contributions are superimposed for the two temperatures up to about $C(CO_2)$ = 6 mol L^{-1}. At higher CO_2 concentrations, we observe a further increase of the area for both the CO_2 and the H_2 contribution but to a lesser extent and in particular at 36°C where a plateau like behavior is observed around $C(CO_2)$ = 10 mol L^{-1}. This last observation could be related to the local density fluctuations that are known to take place near the critical point [28,29,7,12,30,31]. Indeed, such LDE have been put in evidence in supercritical CO_2 by Raman experiments [21] and molecular dynamics simulations [32,33] and are found to be detected as much as the temperature of the fluid is closed to that of the critical temperature. We remember that the critical point of CO_2 is at T_c = 31 °C, P_c = 7.4 MPa and ρ_c = 10.6 mol L^{-1}. Therefore, at 36°C, the LDE are expected to be significant and could explain the plateau like behavior observed at 36°C in the evolution of the CO_2 contribution. At 60°C, the evolution of the area of the CO_2 contribution do not display a significant plateau like behavior in line with the less important expected LDE in supercritical CO_2 at a higher temperature. We remember that as expected from the Beer-Lambert law ($A_i = \varepsilon_i . l . C_i$, with A_i: the measured integrated absorbance of an infrared band associated with the species i (cm^{-1}), ε_i: the molar extinction coefficient of the infrared band ($L.mol^{-1}.cm^{-2}$), l: the thickness of the sample (cm) and C_i: the concentration of the species i ($mol.L^{-1}$)), the evolution of the area of the CO_2 contribution should be directly proportional to the CO_2 concentration. This observation is valid if we consider that the molar extinction coefficient of the CO_2 band of interest is constant over the range of temperature and pressure investigated. Such rule has been demonstrated by the pioneering work of Buback *et al.* [34] showing that the molar extinction coefficient of

combination bands of CO_2 were almost independent of the CO_2 concentration. In order to see to which extent this rule is still valid in our experiments, we have calculated the molar extinction coefficient ε_i from the equation $\varepsilon_i = {A_i}/{l.C_i}$ by using the values of A_i and C_i reported in **Figure 3a** for the two modes of CO_2 at the two different temperatures. The calculated ε_i as a function of the CO_2 pressure are reported in **Figure 3b** for the $4\nu_2 + \nu_3$ and $2\nu_1 + \nu_3$ combination modes of CO_2 for 36 and 60°C. We remember that the ε_i values are related to the transition dipole moment $\delta\mu/\delta Q$ of the vibrational mode under consideration and could be directly compared with infrared intensities calculated by ab-initio methods [35]. At 60°C, we observe a progressive decrease with the CO_2 concentration of the molar extinction coefficient of both combination modes $4\nu_2 + \nu_3$ and $2\nu_1 + \nu_3$ of CO_2 from 1.9 to 1.2 L mol^{-1} cm^{-2} and 2.8 to 2.1 L mol^{-1} cm^{-2} respectively. The same values are obtained at 36°C for low CO_2 concentrations between 1 and 6 mol L^{-1} whereas at higher concentrations, the decrease is more pronounced at 36°C than at 60°C. Therefore, our results are not consistent with the previous results reported by Buback *et al.* However, we emphasize that the results of Buback *et al.* [34] were averaged over a large domain of temperature between 300 and 500 K whereas in this work, the results are reported for given temperatures that are close to the critical temperature. Under these conditions, the general rule proposed by Buback *et al.* is no longer valid for supercritical CO_2 at temperature close to its critical point. Therefore, we believe that the evolution of the molar extinction coefficient of both combination modes can be interpreted as variation of the molecular interactions in the sample that could change over the pressure and temperature of the supercritical fluid and also directly connected to scattering of the medium due to the LDE that exist in the vicinity of the critical point of supercritical CO_2.

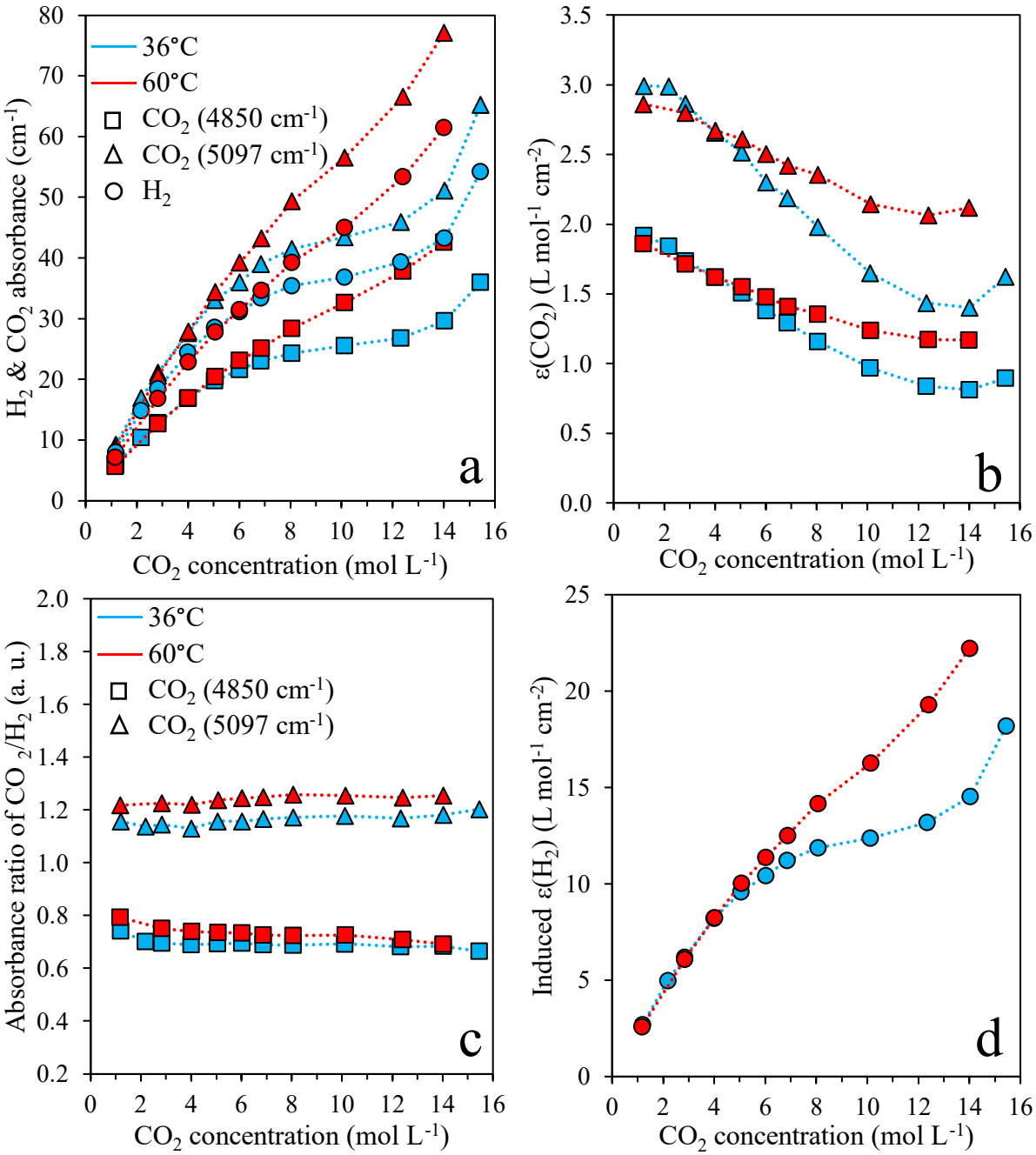

Figure 3: Evolution as a function of the CO_2 concentration at 36 and 60°C of the integrated absorbance of the $4\nu_2 + \nu_3$ (4850 cm^{-1}) and $2\nu_1 + \nu_3$ (5097 cm^{-1}) combination band of CO_2 and of the H_2 peak at 4170 cm^{-1} obtained by IR spectroscopy (a), the molar extinction coefficient of the CO_2 combinations bands (b), the induced molar extinction coefficient associated with the H_2 peak (d) and the absorbance ratio CO_2/H_2 for both combination modes of CO_2 (c).

Regarding the evolution of the IR area of the H_2 contribution in **Figure 3a**, we observed that it follows the same evolution than the CO_2 contribution. Indeed, the ratios of the area of the CO_2 contributions at 4850 and 5097 cm^{-1} over that of the H_2 peak at 4150 cm^{-1} reported in **Figure 3c** are found to be almost constant over the whole range of CO_2 concentration. As the H_2 stretching vibration is inactive in IR spectroscopy, the observed H_2 spectrum in supercritical CO_2 is due to an induced dipole moment on the H_2 molecule that results from its interaction with the surrounding CO_2 molecules. These collision-induced effects have already been

reported for H_2 under high pressure in neat conditions or dissolved in rare gases [13,14]. However, to the best of our knowledge, the collision-induced IR spectrum of H_2 in supercritical CO_2 has not been reported in the literature. Therefore, we have calculated the induced molar extinction coefficient of the H_2 peak at 4150 cm^{-1} from the evolution of its absorbance as a function of the CO_2 pressure knowing that the concentration of H_2 in the mixture is constant (see **Figure 3d**). The molar extinction coefficient of H_2 increases with the CO_2 concentration similarly for the two temperatures up to about $C(CO_2)$=6 $mol.L^{-1}$. At higher CO_2 concentrations, we observe a further increase of the molar extinction coefficient of H_2 but to a lesser extent and in particular at 36°C where a plateau like behavior is observed around $C(CO_2)$ = 10 $mol.L^{-1}$. This last observation could also be related to the local density fluctuations that take place in the vicinity of the critical point of CO_2.

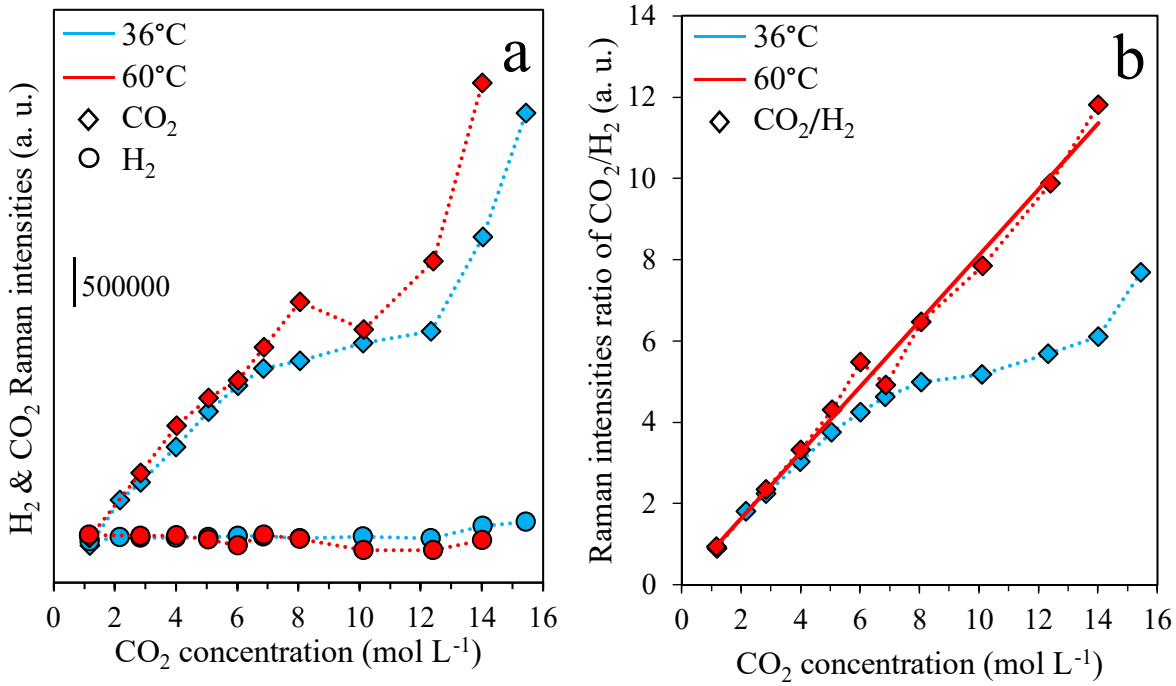

Figure 4: Evolution as a function of the CO_2 concentration at 36 and 60°C of the intensities of the CO_2 Fermi dyad (I_{dyad}) and H_2 rotational mode S1 at 581 cm^{-1} (I_{S1}) obtained by Raman spectroscopy (a) and the intensity ratio $(I_{dyad})/(I_{S1})$ (b)

Regarding the Raman data reported in **Figure 4a**, the area of the CO_2 dyad increases non monotonously with the CO_2 concentration displaying a plateau like behavior observed for the two temperatures around $C(CO_2)$ = 10 $mol.L^{-1}$ as it is observed for the IR spectra. Regarding the area of the H_2 contribution, it remains almost constant regardless of concentration of CO_2 displaying only a weak decrease observed around $C(CO_2)$ = 10 $mol.L^{-1}$. This result is consistent with the fact that the H_2 concentration in the mixture is constant. Therefore, the Raman data are in qualitative agreement with the fact that in our experiments, the H_2 concentration is kept constant while the CO_2 concentration is increased from 1 to 15 $mol.L^{-1}$. Although the non-monotonous evolution of the area of the CO_2 dyad could be also due to the LDE that are predominant around the critical density, Raman intensities are not absolute and depend on many factors (laser and detector stability, fluorescence, Mie diffusion, …). To circumvent the fact that Raman intensities are not absolute, ratio techniques have been proposed in the literature to

obtain quantitative information from Raman spectra in particular for the determination of the solubility of CO_2 in water [36–38]**.** Thus, the CO_2 bands are referenced to the O–H stretching band of water and the calibration curves relating band height (area) ratios to gas concentration are found to be linear over a range of temperatures and pressures. We have applied this methodology to our Raman data and calculated the ratio of the area of the CO_2 bands to that of the S1 band of H_2 whose concentration is constant over the whole range of CO_2 concentration (see **Figure 4b**). At 60°C, a linear increase of the ratio $(I_{dyad})/(I_{S1})$ is observed with the increase of the CO_2 concentration. Thus, it results that the concentration of CO_2 in the H_2-CO_2 mixture can be determined using this methodology as it was applied previously for H_2O-CO_2 mixture. However, at 36°C, we observe a departure from the linearity with a plateau like behavior of the $(I_{dyad})/(I_{S1})$ ratio observed from 8 to 12 mol.L^{-1} of CO_2 and then a further increase at higher concentration with the same slope than that observed at 60°C. This departure from linearity could result from the local density fluctuations that are expected to be more pronounced in the vicinity of the critical point of CO_2.

4- Conclusion

A single high-pressure cell was used for the *in situ* monitoring of H_2 diluted in supercritical CO_2 by co-localized IR/Raman spectroscopies. A constant pressure of H_2 of 3 MPa was applied in the cell heated at 36°C or 60°C and the concentration of CO_2 was increased from 1 to 15 mol.L^{-1}. In the spectral range between 3800 and 5200 cm^{-1}, IR absorption spectra associated with CO_2 combination modes increases almost linearly with the CO_2 concentration from 1 to around 6 mol.L^{-1} for both temperature at 36 and 60°C. Above 6 mol.L^{-1}, the increase of intensities was slow down because of a plateau like behavior that was observed mostly at 36°C compared to the higher temperature of 60°C. The same behavior was observed for the collision-induced stretching mode of H_2 observed at about 4150 cm^{-1} that is reported for the first time in supercritical CO_2. Interestingly, it is found that the ratios of the area of the CO_2 contributions at 4850 and 5097 cm^{-1} over that of the H_2 stretching mode are found to be almost constant over the whole range of CO_2 concentration.

In the spectral range between 300 and 1400 cm^{-1}, Raman scattering spectra associated with the Fermi dyad of CO_2 are found to increase with the CO_2 concentration from 1 to 15 mol.L^{-1} whereas the rotational bands of H_2 remain constant which is in accordance with the constant pressure of H_2. In order to analyze quantitatively the Raman data, the intensity of the rotational mode S1 at 581 cm^{-1} of H_2 was used as an internal standard. At 60°C a linear increase of the ratio $(I_{dyad})/(I_{S1})$ is observed with the increase of the CO_2 concentration, however, a departure from the linearity with a plateau like behavior for this ratio was observed at 36°C from 8 to 12 mol.L^{-1}. Knowing that the critical concentration of CO_2 is at about 10.6 mol.L^{-1}, the non-linear behavior of the evolution of both IR and Raman intensities was related to the local density fluctuations that are significant near the critical point of CO_2. Finally, the use of co-localized IR/Raman spectroscopies allows to reduce experimental errors related to the reproducibility of the experimental conditions (temperature, pressure, homogeneity of the mixture) when independent IR and Raman experiments are performed.

ACKNOWLEDGMENTS

The authors acknowledge the Region Nouvelle Aquitaine and the University of Poitiers for their financial support for the funding of the PhD of I. Bonnin. They are also grateful to the program "Défi in situ en conditions extrêmes" of the MITI of CNRS for the financial support to the infrared and Raman equipment, to INCREASE Federation and to the GDR 2035 SolvATE.

References

[1] L. Plasseraud, Carbon Dioxide as Chemical Feedstock. Edited by Michele Aresta., ChemSusChem. 3 (2010) 631–632. https://doi.org/10.1002/cssc.201000097.
[2] P. Styring, ed., Carbon dioxide utilisation: closing the carbon cycle, Elsevier, Amsterdam Heidelberg, 2015.
[3] P.J.A. Kenis, A. Dibenedetto, T. Zhang, Carbon Dioxide Utilization Coming of Age, ChemPhysChem. 18 (2017) 3091–3093. https://doi.org/10.1002/cphc.201701204.
[4] J. Artz, T.E. Müller, K. Thenert, J. Kleinekorte, R. Meys, A. Sternberg, A. Bardow, W. Leitner, Sustainable Conversion of Carbon Dioxide: An Integrated Review of Catalysis and Life Cycle Assessment, Chem. Rev. 118 (2018) 434–504. https://doi.org/10.1021/acs.chemrev.7b00435.
[5] T.A. Atsbha, T. Yoon, P. Seongho, C.-J. Lee, A review on the catalytic conversion of CO2 using H2 for synthesis of CO, methanol, and hydrocarbons, Journal of CO2 Utilization. 44 (2021) 101413. https://doi.org/10.1016/j.jcou.2020.101413.
[6] P.G. Jessop, T. Ikariya, R. Noyori, Homogeneous catalytic hydrogenation of supercritical carbon dioxide, Nature. 368 (1994) 231–233. https://doi.org/10.1038/368231a0.
[7] S.C. Tucker, Solvent Density Inhomogeneities in Supercritical Fluids, Chem. Rev. 99 (1999) 391–418. https://doi.org/10.1021/cr9700437.
[8] O. Kajimoto, Solvation in Supercritical Fluids: Its Effects on Energy Transfer and Chemical Reactions, Chem. Rev. 99 (1999) 355–390. https://doi.org/10.1021/cr970031l.
[9] K. Nishikawa, T. Morita, Inhomogeneity of molecular distribution in supercritical fluids, Chemical Physics Letters. 316 (2000) 238–242. https://doi.org/10.1016/S0009-2614(99)01241-5.
[10] S.A. Egorov, Local density augmentation in attractive supercritical solutions: Inhomogeneous fluid approach, J. Chem. Phys. 112 (2000) 7138–7146. https://doi.org/10.1063/1.481308.
[11] S.A. Egorov, Preferential solvation in supercritical fluids: An integral equation study, The Journal of Chemical Physics. 113 (2000) 7502–7510. https://doi.org/10.1063/1.1313555.
[12] W. Song, R. Biswas, M. Maroncelli, Intermolecular Interactions and Local Density Augmentation in Supercritical Solvation: A Survey of Simulation and Experimental Results, J. Phys. Chem. A. 104 (2000) 6924–6939. https://doi.org/10.1021/jp000888d.
[13] R. Coulon, L. Galatry, J. Robin, B. Vodar, Sur le spectre infrarouge de H2, induit par le champ intermoléculaire dans les mélanges H2—ClH et dans H 2 pur comprimés, J. Phys. Radium. 16 (1955) 728–729. https://doi.org/10.1051/jphysrad:01955001608-9072800.
[14] H.L. Welsh, The Pressure-Induced Infrared Spectrum of Hydrogen and its Application to the Study of Planetary Atmospheres, Journal of the Atmospheric Sciences. 26 (1969) 835–840. https://doi.org/10.1175/1520-0469(1969)026<0835:TPIISO>2.0.CO;2.
[15] N.O. of D. and Informatics, Bienvenue sur le WebBook de Chimie NIST, (n.d.). https://doi.org/10.18434/T4D303.
[16] R. Span, W. Wagner, A New Equation of State for Carbon Dioxide Covering the Fluid Region from the Triple-Point Temperature to 1100 K at Pressures up to 800 MPa, Journal of Physical and Chemical Reference Data. 25 (1996) 1509–1596. https://doi.org/10.1063/1.555991.
[17] G. Herzberg, Molecular spectra and molecular structure: Infrared and Raman Spectra pf Polyatomic Molecules, D. Van Nostrand Company, Princeton, NJ; Toronto, 1945.
[18] J.V. Kranendonk, Intercollisional interference effects in pressure-induced infrared spectra, Can. J. Phys. 46 (1968) 1173–1179. https://doi.org/10.1139/p68-150.

[19] Y. Garrabos, M.A. Echargui, F. Marsault-Herail, Comparison between the density effects on the levels of the Raman spectra of the Fermi resonance doublet of the 12C16O2 and 13C16O2 molecules, J. Chem. Phys. 91 (1989) 5869–5881. https://doi.org/10.1063/1.457455.
[20] H. Nakayama, K. Saitow, M. Sakashita, K. Ishii, K. Nishikawa, Raman spectral changes of neat CO2 across the ridge of density fluctuation in supercritical region, Chemical Physics Letters. 320 (2000) 323–327. https://doi.org/10.1016/S0009-2614(00)00249-9.
[21] M.I. Cabaço, S. Longelin, Y. Danten, M. Besnard, Local Density Enhancement in Supercritical Carbon Dioxide Studied by Raman Spectroscopy, J. Phys. Chem. A. 111 (2007) 12966–12971. https://doi.org/10.1021/jp0756707.
[22] M.I. Cabaço, S. Longelin, Y. Danten, M. Besnard, Transient dimer formation in supercritical carbon dioxide as seen from Raman scattering, J. Chem. Phys. 128 (2008) 074507. https://doi.org/10.1063/1.2833493.
[23] A. Idrissi, C. Ruckebusch, B. Debus, L. Boussekey, P. Damay, Probing local structure of sub and supercritical CO2 by using two-dimensional Raman correlation spectroscopy, Journal of Molecular Liquids. 164 (2011) 11–16. https://doi.org/10.1016/j.molliq.2011.07.015.
[24] D.K. Veirs, G.M. Rosenblatt, Raman line positions in molecular hydrogen: H2, HD, HT, D2, DT, and T2, Journal of Molecular Spectroscopy. 121 (1987) 401–419. https://doi.org/10.1016/0022-2852(87)90058-0.
[25] R.T. Howie, I.B. Magdău, A.F. Goncharov, G.J. Ackland, E. Gregoryanz, Phonon Localization by Mass Disorder in Dense Hydrogen-Deuterium Binary Alloy, Phys. Rev. Lett. 113 (2014) 175501. https://doi.org/10.1103/PhysRevLett.113.175501.
[26] L. Li, X. Zhang, Z. Luan, Z. Du, S. Xi, B. Wang, L. Cao, C. Lian, J. Yan, Raman vibrational spectral characteristics and quantitative analysis of H_2 up to 400°C and 40 MPa, J Raman Spectrosc. 49 (2018) 1722–1731. https://doi.org/10.1002/jrs.5420.
[27] D.V. Petrov, I.I. Matrosov, D.O. Sedinkin, A.R. Zaripov, Raman Spectra of Nitrogen, Carbon Dioxide, and Hydrogen in a Methane Environment, Opt. Spectrosc. 124 (2018) 8–12. https://doi.org/10.1134/S0030400X18010137.
[28] N. Wada, M. Saito, D. Kitada, R.L. Smith, H. Inomata, K. Arai, S. Saito, Local Excess Density about Substituted Benzene Compounds in Supercritical CO_2 Based on FT-IR Spectroscopy, J. Phys. Chem. B. 101 (1997) 10918–10922. https://doi.org/10.1021/jp972309j.
[29] G. Goodyear, S.C. Tucker, What causes the vibrational lifetime plateau in supercritical fluids?, The Journal of Chemical Physics. 110 (1999) 3643–3646. https://doi.org/10.1063/1.478253.
[30] M.I. Cabaço, M. Besnard, T. Tassaing, Y. Danten, Local density inhomogeneities detected by Raman scattering in supercritical hexafluorobenzene, Pure and Applied Chemistry. 76 (2004) 141–146. https://doi.org/10.1351/pac200476010141.
[31] T. Tassaing, R. Oparin, Y. Danten, M. Besnard, Water–CO2 interaction in supercritical CO2 as studied by infrared spectroscopy and vibrational frequency shift calculations, The Journal of Supercritical Fluids. 33 (2005) 85–92. https://doi.org/10.1016/j.supflu.2004.05.003.
[32] I. Skarmoutsos, J. Samios, Local Density Inhomogeneities and Dynamics in Supercritical Water: A Molecular Dynamics Simulation Approach, J. Phys. Chem. B. 110 (2006) 21931–21937. https://doi.org/10.1021/jp060955p.
[33] I. Skarmoutsos, J. Samios, Local density augmentation and dynamic properties of hydrogen-and non-hydrogen-bonded supercritical fluids: A molecular dynamics study, The Journal of Chemical Physics. 126 (2007) 044503. https://doi.org/10.1063/1.2431370.
[34] M. Buback, J. Schweer, H. Tups, Near Infrared Absorption of Pure Carbon Dioxide up to 3100 bar and 500 K. I. Wavenumber Range 3200 cm^{-1} to 5600 cm^{-1}, Zeitschrift Für Naturforschung A. 41 (1986) 505–511. https://doi.org/10.1515/zna-1986-0308.
[35] D. Begue, I. Baraille, P.A. Garrain, A. Dargelos, T. Tassaing, Calculation of IR frequencies and intensities in electrical and mechanical anharmonicity approximations: Application to small water clusters, J. Chem. Phys., 133 (2010) 034102. https://doi.org/10.1063/1.3457482
[36] S.N. White, Qualitative and Quantitative Analysis of CO2 and CH4 Dissolved in Water and Seawater Using Laser Raman Spectroscopy, Appl Spectrosc. 64 (2010) 819–827. https://doi.org/10.1366/000370210791666354.

[37] N. Liu, C. Aymonier, C. Lecoutre, Y. Garrabos, S. Marre, Microfluidic approach for studying CO2 solubility in water and brine using confocal Raman spectroscopy, Chemical Physics Letters. 551 (2012) 139–143. https://doi.org/10.1016/j.cplett.2012.09.007.
[38] M.-C. Caumon, J. Sterpenich, A. Randi, J. Pironon, Measuring mutual solubility in the H2O–CO2 system up to 200 bar and 100°C by in situ Raman spectroscopy, International Journal of Greenhouse Gas Control. 47 (2016) 63. https://doi.org/10.1016/j.ijggc.2016.01.034.